

# Reconstructing Robot Operations via Radio-Frequency Side-Channel

Ryan Shah  
University of Strathclyde  
United Kingdom  
ryan.shah@strath.ac.uk

Mujeeb Ahmed  
University of Strathclyde  
United Kingdom  
mujeeb.ahmed@strath.ac.uk

Shishir Nagaraja  
Newcastle University  
United Kingdom  
shishir.nagaraja@newcastle.ac.uk

## ABSTRACT

Connected teleoperated robotic systems play a key role in ensuring operational workflows are carried out with high levels of accuracy and low margins of error. In recent years, a variety of attacks have been proposed that actively target the robot itself from the cyber domain. However, little attention has been paid to the capabilities of a passive attacker. In this work, we investigate whether an insider adversary can accurately fingerprint robot movements and operational warehousing workflows via the radio frequency side channel in a stealthy manner. Using an SVM for classification, we found that an adversary can fingerprint individual robot movements with at least 96% accuracy, increasing to near perfect accuracy when reconstructing entire warehousing workflows.

## CCS CONCEPTS

• Security and privacy → Systems security; Side-channel analysis and countermeasures.

## KEYWORDS

robot, security, privacy, radio frequency, side-channel attack, neural network

## ACM Reference Format:

Ryan Shah, Mujeeb Ahmed, and Shishir Nagaraja. 2022. Reconstructing Robot Operations via Radio-Frequency Side-Channel. In *Proceedings of ACM Conference (Conference'17)*. ACM, New York, NY, USA, 10 pages. <https://doi.org/10.1145/nnnnnnn.nnnnnnn>

## 1 INTRODUCTION

Teleoperated robotics systems are becoming more prominent in many applications, in particular surgical [15, 35] and industrial environments [4, 13, 18]. The key reason for their employment pertains to promises of higher efficiency and accuracy, and lower margins of error, compared to a human traditionally operating in the same manner. Many of these robotic systems are Internet-connected, which leaves them vulnerable to attack and compromise in the cyber domain [5, 9, 22]. These attacks vary from manipulating messages and feedback to or from the operator, to directly hijacking the robot's controller directly. However, most of this research focuses

on active attackers, with little focus given to reconnaissance aspects in a passive manner. While active attacks can be deadly to the operating environment and subject(s) involved, passive attacks can result in huge losses that stem from stealthy, unintentional information leakage. For example, if an attacker is able to identify what workflows a robot is carrying out, such as the movement of packages in a warehouse between belts, they could use this information to sell on to competitors that can understand how competing warehousing facilities operate and use this information to a malicious advantage [21, 27].

In this work we seek to explore other mechanisms to passively learn about robotic workflows. Side channels have previously been used in different technological domains as a means to learn sensitive information about the devices, processes and algorithms [6, 32, 34]. One particularly interesting side channel looks at IP theft via the power side channel in 3D printers [11], focusing on predictable movements and reconstructing G-code corresponding to IP. In the case of many robots, however, movement inference is much more dynamic and unpredictable. In this work, we propose a side channel technique to mount an information leakage attack, leveraging unintentional radio frequency (RF) emissions during normal robot operations. While such information could be used to compromise IP, information leakages from robotic workflows as previously described could lead to wholesome compromise of operational confidentiality of organisations. In a typical industrial robot, for example, components such as stepper motors and microprocessors are used which can emanate unintentional radio frequencies [7]. By conducting a feasibility test which explored whether our robot did in fact emit unintentional radio frequencies, given the use of the same components, we found that this was in fact true. We collected samples of RF signals corresponding to both individual robot movements along each of three axes (X, Y and Z) and their permutations, as well as those corresponding to entire warehousing workflows (i.e. picking packages from one location and placing them in another). We then follow a inference technique to extract a small subset of features that represent enough variance to construct an accurate movement or workflow fingerprint. Through the use of an SVM classifier, we observe at least 96% accuracy as a baseline set of results, with similar results observed for more fine-grained information such as how fast or long the robot moves. Further, we show that entire workflows can be reconstructed with even higher accuracy than a pattern-matching approach from individual movements alone.

**Organisation.** This paper is organised as follows. In Section 2, we provide background information on radio frequency and teleoperated robotic systems, and set out the threat model for this attack. We then discuss our attack methodology and evaluate the attack

Permission to make digital or hard copies of all or part of this work for personal or classroom use is granted without fee provided that copies are not made or distributed for profit or commercial advantage and that copies bear this notice and the full citation on the first page. Copyrights for components of this work owned by others than ACM must be honored. Abstracting with credit is permitted. To copy otherwise, or republish, to post on servers or to redistribute to lists, requires prior specific permission and/or a fee. Request permissions from [permissions@acm.org](mailto:permissions@acm.org).  
*Conference'17, July 2017, Washington, DC, USA*

© 2022 Association for Computing Machinery.  
ACM ISBN 978-x-xxxx-xxxx-x/YY/MM...\$15.00  
<https://doi.org/10.1145/nnnnnnn.nnnnnnn>

in Section 3. A discussion on our findings and insights is found in Section 4 with related work provided in Section 5. Finally, we conclude in Section 6.

## 2 BACKGROUND

### 2.1 Radio Frequency

Radio Frequency (RF) is used in a wide array of application contexts, ranging from TV and radio, to wireless and satellite communications. Specifically, it is a measurement which represents the oscillation rate of EMF waves whose frequencies are within range of  $\sim 3\text{kHz}$ – $300\text{GHz}$ , and alternating currents that carry the signal. While the term radio frequency refers to the range of  $3\text{kHz}$ – $300\text{GHz}$ , this is actually the radio spectrum in which several frequency bands are defined in which different transmission systems operate. For example, AM radio operates within  $600\text{kHz}$ – $1.6\text{MHz}$  whilst audible sound waves usually broadcast between  $20\text{Hz}$ – $10\text{kHz}$ .

There are two oscillation types, electrical and mechanical oscillation, however most cases of RF refer to electrical oscillations. Electronic circuits emit some degree of electromagnetic emissions while they operate. While these emissions can theoretically span the entire spectrum, the focus of this study is on emissions that fall within the radio frequency spectrum. While there may be many significant sources of unintentional RF emissions, many robotic systems will make use of microprocessors and stepper motors. The former has been demonstrated to emit RF due to switching activities of transistors alternating varying current flows [7]. Similarly, in the case of the stepper motors, digital pulses and phase shifts in voltage may also contribute to RF emissions.

### 2.2 Teleoperated Industrial Robotic Systems

Teleoperated robotic systems play pivotal roles in safety-critical environments such as surgical theatres and manufacturing facilities, providing high levels of accuracy and precision, and lower margins of error compared to humans performing the same task(s). In industrial settings, notable examples include the likes of robotic arms (and others) in environments such as in production lines [1] and product warehouses [2, 13], among others [12, 17, 19, 36].

While such systems span a variety of environments, they all share a common system architecture [30]. Simply, there exists: a controller (i.e. a teach pendant) which has physical controls or a touch-screen interactive GUI to control the robot; a set of input and output devices (sensors and actuators); and a network in which the robot operates, all linked together via an electronic control system. The primary link in these architectures is that between the controller and electronic control system, and is considered safety-critical due to the ability to directly influence the actions the robot can and will perform. In this paper, we make use of a robotic arm – common to many industrial applications – which consists of three stepper motors for each of the three axes (Figure 1). The base motor controls the Y axis while the left and right control the X and Z axes. In some cases, the microprocessor may be located in another physical component between the robot and controller, however in others it may be situated in the robot itself. In this robot, the microprocessor is located in the base structure alongside the stepper motor. We believe that this robot is a suitable replication candidate for this attack as it compares to other single-arm robots used in



Figure 1: Robot Components

typical industrial settings such as warehouses, which have at least 3 degrees-of-freedom, and also consists of the same principal components for movement fingerprinting (microprocessor and stepper motors). With regard to potential emanations of unintentional RF, the primary component of interest is the microprocessor in the base of the arm robot. However, given that stepper motors may also contribute to sources of RF, these are also of interest to an attacker.

### 2.3 Threat Model

In a teleoperated architecture, many attacks have been presented in literature. These range from tampering with control commands, modifying feedback, and physical-domain attacks (i.e. modifying operational environment), among others [5, 22]. However, most of these attacks focus on an active adversary with little attention paid to passive (weaker) adversaries. In this work, we look at the capabilities of a passive adversary.

The goal in this context is a *stealthy* approach to fingerprint the movements a teleoperated industrial robot can carry out via the radio-frequency side channel. If successful, robot movement fingerprints can be used to not only determine possible workflows, but also be used to reconstruct these workflows. In this work, we look at the context of a logistics warehouse where products are packaged and stored or moved around the warehouses (i.e. along conveyor belts) to then progress to the next stage in a supply chain.

The primary adversary we consider in the scope of this study is an insider, such as technical staff who operate or maintain the robot on the warehouse floor. To capture unintentional RF emissions, an RF receiver is used. These have varying ranges for frequency capture but also can vary in physical size as well. A passive insider here should be stealthy to avoid possible detection, and thus the question pertaining to this is, does there exist a small enough receiver to be used to capture the RF emanations from the robot to minimise the

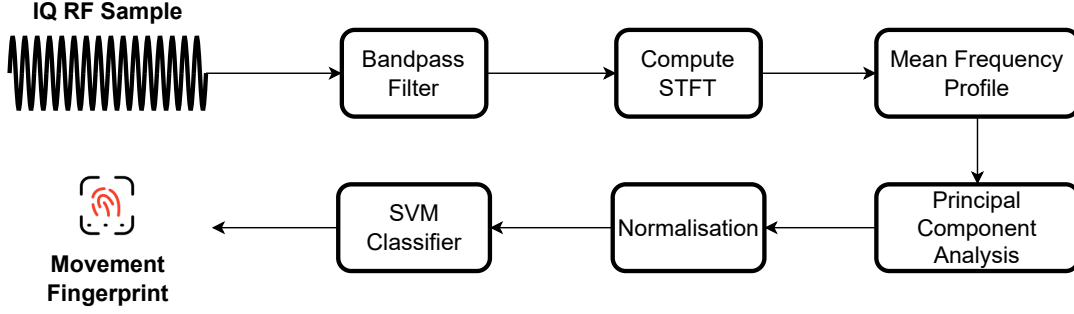


Figure 2: Attack Methodology

possibility of detection. Aside from the ability to conduct the attack, and other important consideration relates to the opportunities that arise from the successful collection of movement fingerprints. By collecting movement fingerprints, it would be possible to correlate a series of movements with known patterns that correspond to warehousing workflows such as picking and placing products between two locations. Furthermore, it may also be possible to reconstruct workflows directly, by capturing the unintentional RF emanations at the time of these workflows and later performing direct workflow classification (as opposed to workflow identification from a collection of movement series). In either case, the information leakage of these operational movements can expose a degree of operational-level detail that may not be otherwise available to this attacker. First, operational confidentiality in terms of claimed efficiency of warehousing procedures or what operations are carried out in the warehouse could be collected and be used as bribery, leaked to competitors, or be used to discredit an organisation at the expense of compromising operational confidentiality. Third, it may also be possible to identify the contents of packages. While gripping or lifting actions alone may not contribute to an increase in unintentional RF emissions, the weight of products may in fact do so. Specifically, heavier weights inherently require more force to be exerted on the robot to lift products and thus require more power to successfully do so, resulting in increased RF emission.

**2.3.1 Hypotheses and Goals.** In this work, we aim to investigate whether it is indeed possible to passively fingerprint teleoperated robot movements via the RF side channel. While we hypothesise that this will be possible, we question the extents to which this is considered a successful attack. Thus, we propose the following research questions:

- ( $R_1$ ) Can an adversary identify teleoperated robot movements via unintentional RF emissions?
- ( $R_2$ ) Can these robot movements be fingerprinted with more granularity? Specifically, does the speed or distance of movement impact the accuracy of fingerprinting?
- ( $R_3$ ) Can *higher-level* warehousing workflows be reconstructed from unintentional RF emissions?
- ( $R_4$ ) Can this attack be performed stealthily, using an RF antenna/receiver that can potentially operate unnoticed?

### 3 ATTACK METHODOLOGY

As previously stated, the goals of this study are to: (a) fingerprint individual movements of an industrial robot arm, and (b) reconstruct warehousing workflows, using the RF side channel (unintentional RF emissions). An overview of our attack methodology can be seen in Figure 2. We first apply a Butterworth bandpass filter to eliminate undesired frequency content. We then compute the Short-Time Fourier Transform (STFT) to represent the frequency content over time and compute the Mean Frequency Profile (MFP) to observe width to frequency peaks and the cadence of robot movements. We then apply Principal Component Analysis (PCA) for dimensionality reduction and normalise the feature sets before fingerprinting. Further detail to each of the steps in our methodology are subsequently described below.

#### 3.1 Experimental Setup

**3.1.1 Robot Environment.** In the first stage of our setup, we discuss our robotics environment. The focus of this study is on teleoperated industrial robots, particularly those used in warehouses. In this architecture, a robot (consisting of sensors, actuators, etc.) is paired with a controller (i.e teach pendant) that is used to send commands or execute pre-programmed actions which the robot can interpret and execute on the factory floor. In our study, we replicate this on a smaller scale, we used uFactory’s uARM Swift Prooperated by an Arduino Mega 2560 running MicroPython. The controller is run on a Windows 10 laptop running the uARM Python (3.8.X) SDK

To capture RF emissions, we used a Mini-Whip Medium-Shortwave Active Antenna which is placed near the base of the robot arm. The antenna amplifies the unintentional RF signal (emitted during robot operations) and transmits this to an RTL-SDR receiver via a shielded coaxial cable. This antenna is suitable for the scale of our robot in this study, with an operating frequency of 10kHz–30MHz and a small physical size of  $113 * 32 * 7mm$ . The small physical size aims to demonstrate that this attack can be conducted stealthily and *hide* by the robot ( $R_4$ ). The RF emissions were captured as IQ files using SDRuno at a sampling rate of 2MHz. An overview of the robot and antenna setup can be seen in Figure 3, including the robot, SDRplay, antenna and pointer towards the controller.

**3.1.2 Movement Dataset.** The next stage of our experimental setup was to create our movement dataset. In this dataset, we have sets of samples which correlate with our objectives and thus, is split

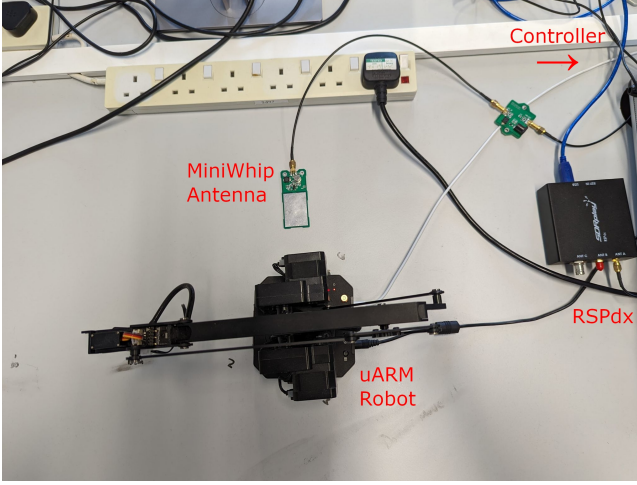


**Figure 3: Robot Environment**

The attack environment consists of the robot, MiniWhip antenna, RSPdx SDR and path to controller

into two subsets. The first subset contains samples pertaining to all permutations of X, Y, and Z with varying speeds of movement (12.5–100mm/s) and distances (1–50mm) ( $R_1 - R_2$ ). The second contains samples of manufacturing workflows ( $R_3$ ) such as pick-and-place, push and pull operations which were replicated from those found in existing industrial robot datasets such as the *Forward Dynamics Dataset Using KUKA LWR and Baxter* [28] for pick and place and the *Inverse Dynamics Dataset Using KUKA* [31] for push/pull. A depiction of these workflows can be seen in Figure 4. We observe that the core information which details these workflows are the dynamic movements being carried out, which are potentially influenced by additional input (i.e. from sensors). As well as this, we also collect samples for pick-and-place operations with packages of different weights (up to maximum load of 1kg for the robot arm), to investigate if content weights can be detected via RF side-channel. Further, also within this second subset, we also perturbed existing data to form additional samples to account for a small degree of entropy that may be present in real-world operations (i.e. those that may arise due to drift in equipment calibration or wear-and-tear). As a whole, the first subset contains ~7.8K samples for individual movements and the second containing ~400 samples for warehousing workflows, with each using 20% of total samples for testing.

### 3.2 Feature Extraction and Movement Fingerprinting

After establishing our movement dataset, the next step in our attack methodology was to extract features from each of the signal samples which would later be used for fingerprinting. The goal here is to ensure that each signal sample for a movement can be easily distinguished from other movements.

First, we wanted to observe whether we could see peaks in the captured RF emissions corresponding to robot movements. To do this, we take the Short-Time Fourier Transform (STFT) of a set of signal samples and compute the log-spectra (spectrogram) using

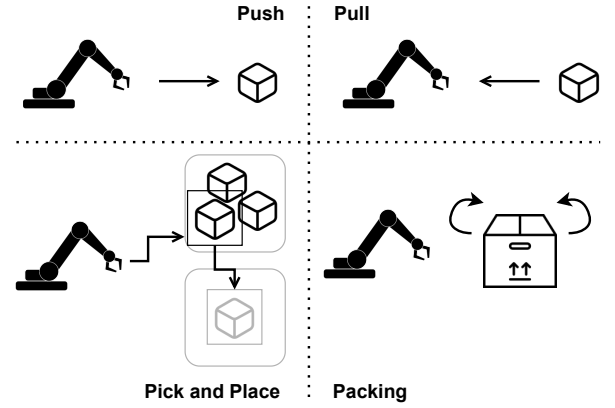


**Figure 4: Depiction of Common Warehousing Workflows**  
Our dataset contains common warehousing workflows such as pushing, pulling, packing and moving objects

a segment length of 8192 and a Hann window as a default, first observation. The STFT allows us to observe information which concerns variations of frequency content of the signal over time. For this, we programmed the robot to perform an X movement at 2s intervals over a period of 10 seconds. As illustrated in Figure 5, we can indeed observe peaks at 2s intervals, which correspond with the robot moving as programmed. However, it is clear that variations present within and between movements are not easily distinguishable through a visual approach. From this, we carry out feature extraction for each sample which will be used as input for movement fingerprinting. The techniques applied for feature extraction are a variation of those presented in the work by Zabalza et al. [39] which demonstrates good classification accuracy for identifying moving targets via radar systems.

First, as shown in Figure 5, we see frequencies drop off after around 500kHz. To confirm this, we look at power spectral density and find that they indeed drop off at around 500kHz and also fall outside a lower limit of ~10kHz. To limit the focus to just the information within these upper and lower bounds, we apply a Butterworth band-pass filter (Figure 6) to filter frequencies out of this range. Interestingly, the filter closely resembles one of decimation due to an observable “flat top” where bins are not scaled relative to one another as would be observed in Gaussian approaches. The Butterworth filter is chosen over other filters given that there is a quicker roll-off at the cut-off frequencies with no rippling and thus robustly preserving frequency content compared to other linear filters.

After applying the band-pass filter, we compute the STFT to obtain the frequency content of our signal samples over time. We then compute the Mean Frequency Profile (MFP) – the mean of the absolute value of each frequency over time – from the STFT. By computing this, we can observe both the location of frequency peaks (variation in amplitude across movements), as well as the width to the frequency peak (different movements may have different velocities for each moving component). The MFP is computed as follows:



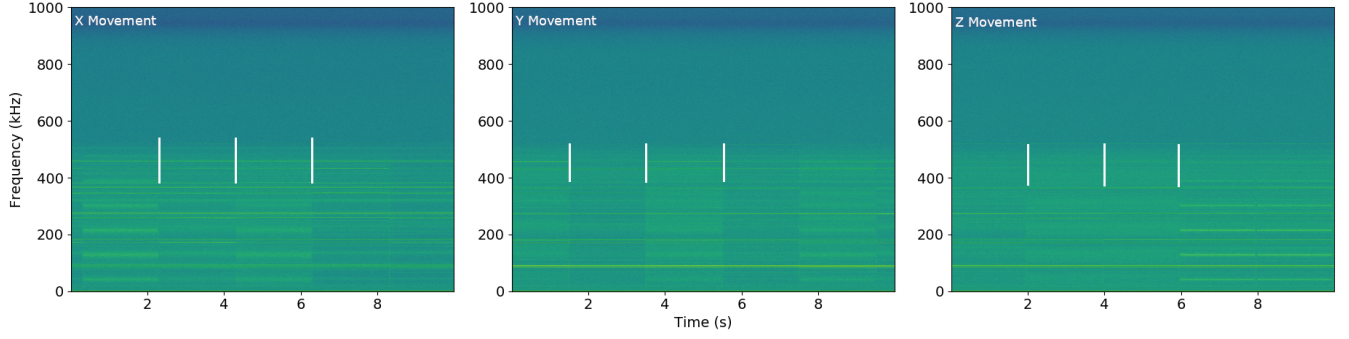


**Figure 5: Observing Frequency Peaks for X, Y and Z Movements**

Observing log-spectra for movements shows movement peaks and demonstrates a visual approach may not be suitable for distinguishing variance within and between movements

$$MFP(v) = \frac{1}{M} \sum_{m=1}^M |STFT(v, m)| \quad MFP(v) \in \mathbb{R}^L \quad (1)$$

where  $M$  is the number of time instants of STFT and  $L$  is the number of discrete points in the Fourier transform. In the case of fingerprinting individual movements, we can assume a constant cadence between target robot movements over windows of time, as they are programmed to be sampled at 2s intervals. By averaging the frequency bins over time, it is possible that some resolution is lost regarding movements of specific components of the robot arm. However, given that the aim is to discriminate between robot movements themselves, rather than parts of the arm, this information is acceptable to discard.

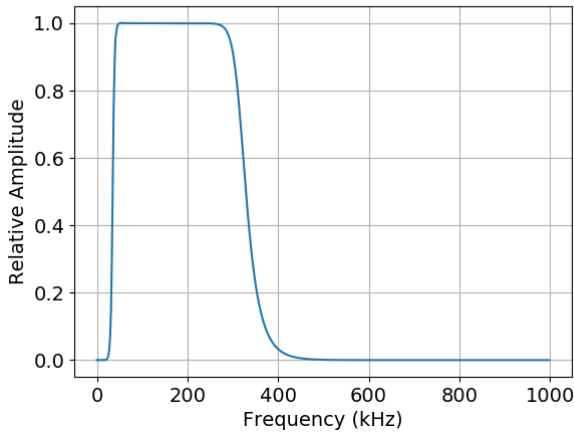


**Figure 6: Butterworth Band-Pass Filter Amplitude Response**

We use the butterworth bandpass filter to eliminate frequencies that fall outside of the range of important frequency content (10–500kHz)

Even by extracting the MFP from the STFT, the resulting feature vector for each movement sample is still fairly large and would

induce a large amount of strain on computing power for fingerprinting. To this, we apply a Principle Component Analysis (PCA) as a dimensionality reduction technique [20] to decorrelate components of the MFP to a smaller subset that still retains a high level of discrimination among features in the feature vector. This allows most of the information to be represented and analysed to produce the same results with a much smaller feature vector. In Figure 7 we can observe the cumulative explained variance among feature vectors for all movements – an accumulation of variance for each principal component. We found that 14 components is enough to represent 99.999% of the overall variation among features.

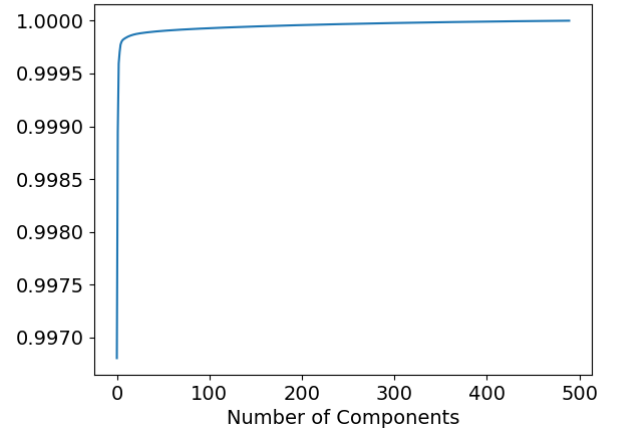


**Figure 7: Cumulative Explained Variance for Movements**

The cumulative explained variance shows that 14 components is enough to represent 99.999% of the overall variation among movements

For the last step in our feature extraction step, we apply normalisation in the form of zero mean and standard unit variance to produce a scaled feature set to optimise the performance in the classification stage.

Once a collection of the resulting feature vectors for our movements are put together in our dataset, we conduct movement classification (fingerprinting) using a C-Support Vector SVM [16, 24] classifier. An SVM was used for this attack, as other approaches such as deep neural networks require a larger sample set and one of the goals of this attack is to conduct it stealthily. Furthermore, the use of an SVM allows for more efficient computation of the movement fingerprints and are easier to train given small datasets. The hyperparameters for the SVM were selected using Grid Search Cross-Validation, which prompted the use of a linear kernel with most optimal kernel parameters of  $\gamma = 1.0e - 4$  and  $C = 1.0e5$ . In this work, for each movement, we have a minimum of 100 samples for each parameter, to which we evaluate whether fingerprinting can be successful with a small sample size and quick sample collection phase for the adversary. In the case of larger sample sizes, other approaches such as SVM trained with Stochastic Gradient Descent (SGD) may be more desirable in terms of computational efficiency [23].

**3.2.1 Choice of STFT Parameters.** Before an evaluation of our attack, the first step is to evaluate a choice of parameters used in the STFT step of the feature extraction process. Specifically, we look at the FFT length and STFT windowing function. Given that our RF samples are recorded at 2MHz sampling rate, we have a signal recorded at 2,000,000 samples per second. According to the Nyquist-Shannon Sampling Theorem [29], this means our signals can contain frequency content up to 1MHz. Given that the STFT provides time-localised frequency content, there is to be a trade-off between temporal and frequency resolution. Simply, a narrow window results in better temporal resolution but poorer frequency resolution, and vice-versa. Given that we are attempting to both discriminate between what movements are being carried out, as well as full operational workflows, it is important to ensure a balance between both temporal and frequency resolutions to allow for success in both cases. Aside from the accuracy as a choice of this first parameter, another consideration is the time taken to compute it. As with most signal processing applications, a relatively fast computation time is desirable, and inherently a longer FFT takes more time to compute. Finally, the last determining factor for the choice of STFT is the windowing function. The use of the (sliding) window function allows for the overlapping of disjointed parts of the input signal. This aims to decrease the amount of spectral leakage and minimise effects such as rippling, by determining the amplitude of side lobes to distribute spectral leakage. A typical window suitable to many applications is the Hann window, which is a form of generalised cosine window, with other popular choices including Hamming and Blackman windows [26]. In this work, we evaluate 3 generalised cosine windows – specifically, the Hann, Hamming and Blackman windows – due to demonstrable success in pulse shaping/filtering [37] and many other applications. Interestingly, given a pre-computed window (as is possible with our relatively constant cadence in movement samples), the window function should not have any impact on computation time, but we evaluate this for completeness.

In Table 1, we can observe the accuracy of a baseline set of results (distance of 1 and lowest speed of 12.5mm/s) with various window functions, FFT lengths and the time taken to compute the STFT

over 100 runs. With respect to the overall accuracy corresponding to window choice, we found that the Hann and Hamming windows both outperformed the Blackman window, with the Hann window having slightly higher accuracy overall. Notably, the accuracy increases as the FFT length increases. A higher FFT length results in a higher spectral resolution but takes longer to compute. Because of this, a key consideration is the computation time for movement fingerprints. With respect to the computation time, we found that the most reasonable window and FFT length is a Hann window with an FFT length of 16384. While the window function has no measurable impact on computation time assuming a pre-computed window, as in our case, we account for erroneous times due to measurement noise. In this case, more bespoke devices such as an FPGA may provide better accuracy for measuring computation time. In either case, with regard to FFT length, a longer window requires a more expensive FFT and ultimately results in a non-linear increase of computation time with length. For this study, a Hann window with FFT length of 16384 is the best choice, as a compromise of 2ms computation time is reasonable for the accuracy increase in comparison with the same FFT length and a Hamming window.

### 3.3 Attack Results

As per our research questions in Section 2.3.1, our evaluation of the results for our proposed attack will be in this order.

**3.3.1 Individual Movement Fingerprints.** As per our first research question, we initially investigate whether the proposed adversary can fingerprint individual robot movements via unintentional RF emissions. Simply, this will formulate a baseline set of results, consisting of a baseline (smallest) distance of 1mm and speed of 12.5mm/s, to which we can compare against other parameters (i.e. movement distance). For all future parameter comparisons, the baseline results in tables are highlighted in gray. As shown in Table 2, we observe an average accuracy of 95% for the baseline. While most movements show relatively consistent accuracy of at least 94%, among them we found that the YZ movement was the lowest at 91% with a small set of samples mistaken for XYZ. Interestingly, the Z movement shows the most success in terms of fingerprinting. Ultimately, it is clear that Y-involved movements show the lowest accuracy. This may be due to the fact that the base motor that handles the Y axis is also situated alongside the microprocessor, such that the mixing of similar frequency ranges may interfere with one another causing a lack in variation.

**3.3.2 Impact of Movement Distance on Fingerprinting.** The second objective concerns a higher level of granularity for movement fingerprints. Specifically, can an adversary infer how far or how fast a movement is being carried out? The first of these two parameters that we evaluate is the distance of movement and how it impacts classification accuracy. The results of this parameter can be seen in Table 2. An overview of these results suggest that fingerprinting is more successful on average as the distance of movement increases, with the exception of the YZ movement. At 2 distance units, we can observe a decrease in precision for most movements, with the exception of Z, XY and XYZ movements. This is potentially due to lowered variation among principle components between 1 and 2 distance units. At 5 distance units, we see much better precision

	Blackman			Hamming			Hann		
	8192	16384	32768	8192	16384	32768	8192	16384	32768
<b>Accuracy</b>	93%	93%	94%	92%	95%	89%	94%	96%	95%
<b>Time (ms)</b>	507	581	740	506	563	646	524	565	655

**Table 1: Comparison of STFT Parameters**

We observe that the Hann window with FFT length of 16384 is the most optimal in terms of accuracy but also efficiency in computing the movement fingerprint

Movement	Distance (mm)					
	1	2	5	10	25	50
<b>X</b>	100%	100%	100%	89%	100%	100%
<b>Y</b>	93%	81%	89%	73%	100%	96%
<b>Z</b>	100%	100%	93%	93%	100%	100%
<b>XY</b>	89%	100%	67%	100%	100%	100%
<b>XZ</b>	100%	88%	100%	100%	100%	92%
<b>YZ</b>	95%	80%	50%	85%	88%	92%
<b>XYZ</b>	94%	88%	62%	87%	88%	96%
<b>Accuracy</b>	96%	91%	78%	89%	96%	96%

**Table 2: Impact of Movement Distance on Classification Accuracy**

Movement distance provides more fine-grained information leakage and can be fingerprinted with similar accuracy to the baseline. Smaller distances have reduced accuracy likely due to similar levels of unintentional RF emissions

compared to 1 or 2 distance units, except for the YZ movement which decreases by 3%. Interestingly, the XY movement also decreases again compared to 2 distance units but to similar precision as the baseline. The YZ movement in this case is incorrectly predicted as other Y-involved movements, with most being the XYZ movement. This same pattern is also observed for the XY movement. At 10 distance units, we observe perfect precision for all movements, with the exception of YZ which has no change compared to 5 units. At 25 distance units, we observe similar precision as with 10 units, however the precision reduces for the XZ and XYZ movements. The YZ movement increases only slightly. Finally, at 50 distance units, the precision increases back to 100% for XZ and increases slightly for the XYZ movement compared to 25 units. Overall, we found that while distance does on average increase the accuracy of movement fingerprinting, larger distances show better success.

**3.3.3 Impact of Movement Speed on Fingerprinting.** As well as movement distance, the speed at which the movement is being carried out may also provide a higher level of granularity to movement fingerprints. The results for the speed parameter can be seen in Table 3. Overall, it is clear that as the speed of movement increases, the variation in the RF feature set reduces resulting in lowered classification accuracy. We observe better fingerprinting accuracy for the XZ movement in the speed parameter compared to the distance parameter. Taking all movements into account, the precision for the Y-involved movements are among the poorest

Movement	Speed (mm/s)				
	12.5	25	50	75	100
<b>X</b>	100%	100%	100%	100%	96%
<b>Y</b>	93%	83%	58%	58%	54%
<b>Z</b>	100%	92%	100%	97%	100%
<b>XY</b>	89%	70%	47%	68%	63%
<b>XZ</b>	100%	100%	97%	97%	97%
<b>YZ</b>	95%	58%	76%	55%	57%
<b>XYZ</b>	94%	69%	70%	70%	45%
<b>Accuracy</b>	96%	84%	85%	80%	77%

**Table 3: Impact of Movement Speed on Classification Accuracy**

Movement speed provides lowered accuracy as the speed increases for movement fingerprints, particularly among Y-based movements, which may be linked to the physical infrastructure

as the speed increases, with many incorrectly predicted as either Y or YZ movements perhaps due to a lack in variation between them. This may be due to the design of the uARM robot in which Y movements making primary use of the base motor (with the X and Z axes primarily using the right and left motors as their respective primary motors). The distance parameter is more accurately fingerprintable than the speed parameter, and thus would be more useful to track. While speed may be a useful candidate still, keeping track of the distance is a more reliable metric in most cases. For example, the speed at which an operator performs an operation can vary depending on the context or object being moved, but the distance may be relatively consistent for these specific avenues. In an industrial setting, for fingerprinting alone speed may not be as useful, however in the case of an audit in which one might wish to determine whether the robot was behaving in an erratic fashion, speed data might prove useful through continuous monitoring.

**3.3.4 Workflow Reconstruction.** Aside from exploring the efficacy of the attack on individual and combinations of movements, which can be used in pattern-based reconstruction, it is also interesting to determine whether higher-level warehousing workflows can be reconstructed via the RF side channel. For this experiment, the second dataset containing warehousing workflow samples was used, which is detailed in Section 3.1.2. The results for the experiment on reconstructing warehousing workflows can be seen in Table 4. In this experiment, three different sets of each workflow were captured

Operation	Recovery Rate		
	1	2	3
Push	100%	100%	100%
Pull	100%	100%	100%
Pick-and-Place	100%	100%	100%
Packing	100%	57%	57%
<b>Accuracy</b>	100%	88%	88%

**Table 4: Workflow Reconstruction Results**

Common warehousing workflows can be reconstructed in their entirety with much higher accuracy, compared to an approach which involves pattern-matching using individual movement fingerprints

and analysed using the same attack strategy as individual movements. Interestingly, looking at the cumulative explained variance of the principal components for workflows, a very similar amount of variance as with individual movements can also be captured for entire workflows with the same number of principal components, and thus the attack remains the same. Using the same SVM parameters, we found that the first set of workflows achieves perfect reconstruction accuracy. While this is a notable result, the second and third sets of these workflows achieves similar results, with the packing operation being the exception with 57% accuracy in both cases. In the case of the second set, some of the pull operations are incorrectly predicted as packing, and for the third set, some samples of pick and place are incorrectly predicted as packing. This may be due to the fact that the packing operation may have similarities to these movements in the sets explored resulting in the lowered accuracy. Overall, it is clear that using this attack approach, an adversary can very successfully reconstruct entire operational workflows. Through the use of continuous monitoring, entire daily operations and their performance (i.e. by also capturing timing information) can be leaked to competitors for a potentially malicious advantage.

## 4 DISCUSSION

Our proposed side channel attack using radio frequency (RF) demonstrates a feasible approach for an insider attacker, such as a malicious technician/operator, to place an easily disguised and economical antenna on the factory floor. By doing so, they can fingerprint robot movements and reconstruct entire warehousing workflows with very high accuracy. Furthermore, our evaluation shows that such an attacker can also infer more fine-grained information such as the speed or distance in which a movement is being carried out.

### 4.1 Defences

Given that the radio frequencies that are captured in this attack are emitted from an unintentional radiator source, in this case the robot, the radiated fields require a form of mitigation (suppression) to prevent information leakage. To recap, the robot used in this study is likely to emit unintentional RF from its microprocessor and stepper motors, with the majority from the microprocessor. A best defence here comes in the form of physical layer security measures such as shielding critical portions of the microprocessor

layout or robot enclosure. Shielding against electromagnetic fields (EMF) such as RF makes use of a barrier made of conductive or magnetic materials to isolate minimise interference but also act as a sort of Faraday cage. The materials typically used include copper, silver or brass, with copper being the most common for RF shielding. In the case of our robot used, the enclosure is made of aluminium. While this is not as conductive as copper (~60%), it is usually a second choice due to other properties such as electrical conductivity, strength-to-weight ratio, cost and malleability. With respect to the enclosure, a suitable defence strategy to explore is to evaluate whether a thicker aluminium casing would provide better protection against the proposed RF side channel attack. Furthermore, it would also be interesting to observe whether other casing materials such as copper or brass might perform with their innate contrasts in protective properties (i.e. conductance).

### 4.2 Impact

While we demonstrate the impact of this attack from a business perspective, in the form of operational compromise of robotic workflows that could leak sensitive business information, it is important to look at the impact of our attack in other areas such as government/international specification, regulations and international standards.

The first impact we look at is government specification. In the United States of America, the government and NATO specification TEMPEST is used to cover methods for eavesdropping on and protecting (shielding) against information leakages from unintentional emanations such as RF or acoustic. While many specifics of TEMPEST are classified, in the public domain three levels of protection requirements are set out: NATO SDIP-27 LEVEL A, B and C. Level A is the strictest standard which assumes the attacker has almost immediate access to the environment or devices. Level B assumes the attacker cannot be within 20 metres and is more relaxed, and Level C assumes a distance of 100 metres. Unfortunately, TEMPEST mainly addresses nation-state level equipment and facilities. The guidance states that in general, devices such as these robots are typically not qualified under TEMPEST as most of these devices, including commercial off-the-shelf components of robots which are assumed to conform to Level C without any modification. Further, it is not clear on specific key requirements of shielding against unintentional emanations. Given the impact on businesses in any respect, their confidentiality is key – particularly against those which they are in conflict (competition) with – and thus the potential of insider threat should ultimately be a cause to improve the standards of robot protection in non-military settings.

The next impact of this attack pertains to regulation and regulatory compliance. Guidance from regulators such as Ofcom in the UK and TÜV issue rules for compliance for all uses of RF, whether emanations occur under normal conditions or from unintentional radiators such as the context of this work. However, such guidance does not cover robotics systems but only a subset of typical components (i.e. power input or cables). In the case of Ofcom, regulation only detail where an EMF record is not required but does not include where robotics systems or unintentional RF emanations apply. Clearly some modifications and additions to existing regulation is needed to cover attacks like this on robotic systems. As well as



existing regulation, one key question that may arise is how can one audit a robot? While continuous monitoring and audits of software and hardware components can provide some guarantees, the risk of malware or invalid device calibration that disrupts operational accuracy also needs attention. Interestingly, we observed that from the high recovery rates of industrial warehousing workflows, the use of the RF side channel can act as a defence that can provide information to auditing procedures. By monitoring typically correct robot workflows over time, any drift in accuracy from either a malicious or unintentional *attack* vector could be recognised by the system, for example through the use of LSTM networks and RF time-series information. This is a point of future work.

Finally, we look at international standards. The key international standard that applies to the impact of this attack is CISPR 11 for governing EMF emissions from industrial, scientific or medical (ISM) equipment, among others, which can use the ISM license free bands like 2.4 GHz. The ISM bands are defined by international telecommunication union (ITU) radio regulations, which have a variety of allocated ranges within the band of  $\sim 6.76\text{MHz}-256\text{GHz}$ . In the context of this attack, we find that our smaller robot falls outside of ISM bands where such standards and regulation typically apply. However, for larger industrial robots, an evaluation of this attack would be worth observing to truly understand the impact in this case. Interestingly, an investigation into the RF emissions related the size and general load/power requirements of different robotic systems may also reveal that some may also fall out of the ISM bands and may in future provoke a discussion on updating existing standards.

### 4.3 Limitations

One limitation of this work is the robot used. In terms of direct replicability for a real-world industrial robot arm, our robot is much smaller than one typically seen on the factory floor. While the attack may not provide the same level of movement inference in this case as with our robot, a larger robot would employ more motors that require more power to operate. Given that the motors and integrated circuits still emit unintentional RF from the nature of their operation [7], the attack would simply require extra exploratory analysis in terms of the frequency range of the RF emissions to tune the parameters. As well as this, it would be interesting to perform an exploratory analysis of unintentional RF emissions from a range of different robots.

A second limitation one can consider is a disconnect between the tool equipped at the end-effector and the motion being carried out. The robot arm used in this study is equipped with an integrated pump with a maximum pressure of 33kPa and maximum lifting weight of 1kg. The goal with the use of the tool was to determine whether an attacker could identify the contents (by weight inference) of packages being lifted. Unfortunately, there was no measurable unintentional RF emissions between weights being lifted, nor to distinguish whether the pump was on or off. For a larger robot however, a pump end-effector with a larger lifting weight that requires more power may change this result. As well as this, it would be interesting to see the impact of additional power requirements for lifting weights with different tools (i.e. grippers) has on RF emissions. One potential solution to this limitation in the

case of our robot could be a different side channel. For example, the acoustic side channel may be useful with measuring the acoustic emanations for lifting heavier weights. Given that heavier weights require more force to lift, and ultimately more power, there may also be more sound emitted as the object is being lifted.

## 5 RELATED WORK

While there have not been any side channel literature pertaining directly to robotics systems, the use of side channels have shown success relating to components of robotics systems, as well as similar architectures such as 3D printers. In this section we present related work on RF side channels and other side channels and techniques related to systems that share common characteristics with robotic systems.

There are many devices which emanate unintentional RF, including microprocessors and motors, among others. Graham et al. [14] demonstrate that RF emanations can be identified by correlating RF emissions with bit flips that produce detectable electrical pulses. This is analogous to the switching activities in transistors as pointed out by Cobb et al. [7]. In similar work, deep learning approaches have shown success operating on raw waveforms [25, 33], such as the use of convolutional neural networks operating on time series data [3, 8] or residual neural networks [38], to fingerprint IoT devices and processes running on them. However, while these approaches are successful, our attack requires a much smaller sample set to show similar accuracy.

Aside from the radio-frequency side channel, other side channels such as power and acoustics also show some success. For example, Sami et al. [32] describe an attack via the acoustic side channel that can extract sound traces from the vibrations reflected to lidar sensors. Several authors [6, 10] propose an acoustic side channel attack on 3D printers wherein acoustic emanations are used to reconstruct G-code used by 3D printers which may correspond to potentially confidential (patented) designs. Related to this, Song et al. [34] also describe a similar end goal but enhancing the acoustic side channel using the magnetic side channel by exploiting the conductivity of a stepper motor. Compared to our work, the extraction of G-code corresponds to Arduino-based 3D printers. Given that our robot is also operated by an Arduino, we show that our attack focuses solely on the movement of the robot arm and thus reconstruction of G-code to then compromise operational confidentiality is an unnecessary extra step. While earlier approaches make use of regression models, more recent work make use of neural networks that require a large labelled sample set to which our approach shows better opportunities for an insider attacker. As well as this, given that individual movements can also be reconstructed, pattern matching individual or permutations of these movements could also lead to the leakage of confidential intellectual property.

## 6 CONCLUSION

In conclusion, we showcase a novel attack on robotic systems that can leak information about confidential warehousing (industrial) workflows via a radio frequency side channel. Instead of a deep learning approach, our attack requires a much smaller sample set

and demonstrates fingerprinting accuracy, of individual robot movements as well as entire workflows, similar to attacks using neural networks. Furthermore, we show that even more fine-grained movements can be inferred from the RF side channel, such as distinguishing the distance or speed a movement is carried out with.

## ACKNOWLEDGMENTS

The authors are grateful for the support by the Engineering and Physical Sciences Research Council (11288S170484-102) and the support of the National Measurement System of the UK Department of Business, Energy & Industrial Strategy, which funded this work as part of NPL's Data Science program.

## REFERENCES

- [1] Doris Aschenbrenner, Michael Fritscher, Felix Sittner, Markus Krauß, and Klaus Schilling. 2015. Teleoperation of an industrial robot in an active production line. *IFAC-PapersOnLine* 48, 10 (2015), 159–164.
- [2] Jose Luis Ordoñez Avila, Hector Jimenez, Tania Marquez, Carlos Muñoz, Alberto Max Carrasco, Maria Elena Perdomo, David Míselem, and David Nolasco. 2020. Study Case: Teleoperated Voice Picking Robots prototype as a logistic solution in Honduras. In *2020 5th International Conference on Control and Robotics Engineering (ICCRE)*. IEEE, 19–24.
- [3] Shaojie Bai, J Zico Kolter, and Vladlen Koltun. 2018. An empirical evaluation of generic convolutional and recurrent networks for sequence modeling. *arXiv preprint arXiv:1803.01271* (2018).
- [4] Michal Bartoš, Vladimír Bulej, Martin Bohušik, Ján Stanček, Vitalii Ivanov, and Peter Macek. 2021. An overview of robot applications in automotive industry. *Transportation Research Procedia* 55 (2021), 837–844.
- [5] Tamara Bonaci, Jeffrey Herron, Tariq Yusuf, et al. 2015. To make a robot secure: An experimental analysis of cyber security threats against teleoperated surgical robots. *arXiv preprint arXiv:1504.04339* (2015).
- [6] Sujit Rokka Chhetri, Arquimedes Canedo, and Mohammad Abdullah Al Faruque. 2017. Confidentiality breach through acoustic side-channel in cyber-physical additive manufacturing systems. *ACM Transactions on Cyber-Physical Systems* 2, 1 (2017), 1–25.
- [7] William E Cobb, Eric W Garcia, Michael A Temple, Rusty O Baldwin, and Yong C Kim. 2010. Physical layer identification of embedded devices using RF-DNA fingerprinting. In *2010-Milcom 2010 Military Communications Conference*. IEEE, 2168–2173.
- [8] Zhicheng Cui, Wenlin Chen, and Yixin Chen. 2016. Multi-scale convolutional neural networks for time series classification. *arXiv preprint arXiv:1603.06995* (2016).
- [9] Nicholas DeMarinis, Stefanie Tellex, Vasileios P Kemerlis, et al. 2019. Scanning the internet for ros: A view of security in robotics research. *2019 International Conference on Robotics and Automation (ICRA)*, 8514–8521.
- [10] Mohammad Abdullah Al Faruque, Sujit Rokka Chhetri, Arquimedes Canedo, et al. 2016. Acoustic side-channel attacks on additive manufacturing systems. *2016 ACM/IEEE 7th international conference on Cyber-Physical Systems (ICCPS)*, 1–10.
- [11] Jacob Gatlin, Sofia Belikovetsky, Yuval Elovici, Anthony Skjellum, Joshua Lubell, Paul Witherell, and Mark Yampolskiy. 2021. Encryption is Futile: Reconstructing 3D-Printed Models Using the Power Side-Channel. In *24th International Symposium on Research in Attacks, Intrusions and Defenses*. 135–147.
- [12] Satoru Goto, Takuya Naka, Yoshitaka Matsuda, and Naruto Egashira. 2010. Teleoperation System of Robot arms combined with remote control and visual servo control. In *Proceedings of SICE Annual Conference 2010*. IEEE, 1975–1981.
- [13] Andrzej Grabowski, Jarosław Jankowski, and Mieszko Wodzyński. 2021. Teleoperated mobile robot with two arms: the influence of a human-machine interface, VR training and operator age. *International Journal of Human-Computer Studies* 156 (2021), 102707.
- [14] James T Graham, Ronald Riley, Rusty Baldwin, and Ashwin Fisher. 2018. Block-level algorithm classification based on RF side-channel. In *Cyber Sensing 2018*, Vol. 10630. SPIE, 44–50.
- [15] Blake Hannaford, Jacob Rosen, Diana W Friedman, et al. 2012. Raven-II: an open platform for surgical robotics research. *IEEE Transactions on Biomedical Engineering* 60 (2012), 954–959. Issue 4.
- [16] Chuanxia Jian, Jian Gao, and Yinhui Ao. 2016. A new sampling method for classifying imbalanced data based on support vector machine ensemble. *Neuro-computing* 193 (2016), 115–122.
- [17] Kaveh Kamali, Ilian A Bonev, and Christian Desrosiers. 2020. Real-time motion planning for robotic teleoperation using dynamic-goal deep reinforcement learning. In *2020 17th Conference on Computer and Robot Vision (CRV)*. IEEE, 182–189.
- [18] N Vimal Kumar and C Selva Kumar. 2018. Development of collision free path planning algorithm for warehouse mobile robot. *Procedia computer science* 133 (2018), 456–463.
- [19] Chunxu Li, Chenguang Yang, Jian Wan, Andy SK Annamalai, and Angelo Cangelosi. 2017. Teleoperation control of Baxter robot using Kalman filter-based sensor fusion. *Systems Science & Control Engineering* 5, 1 (2017), 156–167.
- [20] Ji Ma and Yuyu Yuan. 2019. Dimension reduction of image deep feature using PCA. *Journal of Visual Communication and Image Representation* 63 (2019), 102578.
- [21] Federico Maggi, Davide Quarta, Marcello Pogliani, Mario Polino, Andrea M Zanchettin, and Stefano Zanero. 2017. Rogue robots: Testing the limits of an industrial robot's security. *Trend Micro, Politecnico di Milano, Tech. Rep* (2017), 1–21.
- [22] Jarrod McClean, Christopher Stull, Charles Farrar, et al. 2013. A preliminary cyber-physical security assessment of the robot operating system (ros). *Unmanned Systems Technology* XV 8741, 874110.
- [23] Aditya Krishna Menon. 2009. Large-scale support vector machines: algorithms and theory. *Research Exam, University of California, San Diego* 117 (2009).
- [24] J Novakovic and A Veljovic. 2011. C-support vector classification: Selection of kernel and parameters in medical diagnosis. In *2011 IEEE 9th international symposium on intelligent systems and informatics*. IEEE, 465–470.
- [25] Aaron van den Oord, Sander Dieleman, Heiga Zen, Karen Simonyan, Oriol Vinyals, Alex Graves, Nal Kalchbrenner, Andrew Senior, and Koray Kavukcuoglu. 2016. Wavenet: A generative model for raw audio. *arXiv preprint arXiv:1609.03499* (2016).
- [26] Prajoy Podder, Tanvir Zaman Khan, Mamdudul Haque Khan, and M Muktadir Rahman. 2014. Comparative performance analysis of hamming, hanning and blackman window. *International Journal of Computer Applications* 96, 18 (2014).
- [27] Marcello Pogliani, Davide Quarta, Mario Polino, Martino Vittone, Federico Maggi, and Stefano Zanero. 2019. Security of controlled manufacturing systems in the connected factory: the case of industrial robots. *Journal of Computer Virology and Hacking Techniques* 15, 3 (2019), 161–175.
- [28] Athanasios S Polydoros and Lazaros Nalpanitidis. 2016. A reservoir computing approach for learning forward dynamics of industrial manipulators. In *2016 IEEE/RSJ International Conference on Intelligent Robots and Systems (IROS)*. IEEE, 612–618.
- [29] Emiel Por, Maaike van Kooten, and Vanja Sarkovic. 2019. Nyquist–Shannon sampling theorem. *Leiden University* 1 (2019), 1.
- [30] Davide Quarta, Marcello Pogliani, Mario Polino, Federico Maggi, Andrea Maria Zanchettin, and Stefano Zanero. 2017. An experimental security analysis of an industrial robot controller. In *2017 IEEE Symposium on Security and Privacy (SP)*. IEEE, 268–286.
- [31] Elmar Rueckert, Moritz Nakatenus, Samuele Tosatto, and Jan Peters. 2017. Learning inverse dynamics models in o(n) time with lstm networks. In *2017 IEEE-RAS 17th International Conference on Humanoid Robotics (Humanoids)*. IEEE, 811–816.
- [32] Sriram Sami, Yimin Dai, Sean Rui Xiang Tan, Nirupam Roy, and Jun Han. 2020. Spying with your robot vacuum cleaner: eavesdropping via lidar sensors. In *Proceedings of the 18th Conference on Embedded Networked Sensor Systems*. 354–367.
- [33] Asanka Sayakkara, Nhien-An Le-Khac, and Mark Scanlon. 2019. Leveraging electromagnetic side-channel analysis for the investigation of IoT devices. *Digital Investigation* 29 (2019), S94–S103.
- [34] Chen Song, Feng Lin, Zhongjie Ba, Kui Ren, Chi Zhou, and Wenyao Xu. 2016. My smartphone knows what you print: Exploring smartphone-based side-channel attacks against 3d printers. In *Proceedings of the 2016 ACM SIGSAC Conference on Computer and Communications Security*. 895–907.
- [35] Ashutosh Tewari, James Peabody, Richard Sarle, et al. 2002. Technique of da Vinci robot-assisted anatomic radical prostatectomy. *Urology* 60 (2002), 569–572. Issue 4.
- [36] Juan S Toquica, Diego Benavides, and José Mauricio ST Motta. 2019. Web compliant open architecture for teleoperation of industrial robots. In *2019 IEEE 15th International Conference on Automation Science and Engineering (CASE)*. IEEE, 1408–1414.
- [37] A Vigil, M Belkeldid, and D Malocha. 1993. Application of classical cosine series window functions to full response signaling offset quadrature binary modulation systems. *IEEE transactions on communications* 41, 1 (1993), 11–15.
- [38] Miller L Wilt, Megan M Baker, and Stergios J Papadakis. 2020. Toward an RF side-channel reverse engineering tool. In *2020 IEEE Physical Assurance and Inspection of Electronics (PAINE)*. IEEE, 1–7.
- [39] Jaime Zabalza, Carmine Clemente, Gaetano Di Caterina, Jinchang Ren, John J Soraghan, and Stephen Marshall. 2014. Robust PCA micro-Doppler classification using SVM on embedded systems. *IEEE Trans. Aerospace Electron. Systems* 50, 3 (2014), 2304–2310.